Supporting Information

Vogel et al. 10.1073/pnas.0914720107

SI Text

SI Materials and Methods. ***Device assembly.*** The operation and performance of the MS and SW devices are very similar despite differences in assembly. In both cases a pumping layer is sandwiched between the top plate and bottom plate. SW devices are permanently held together and sealed by a bead of epoxy around the perimeter (note the lateral offset between top and bottom plates in Fig. 2*A* to aid in assembly). MS devices (Fig. 1*B*) are assembled with several rubber gaskets and clamped together with screws.

For proper operation of the switchable electronically-controlled capillary adhesion device (SECAD), care must be taken during design and assembly to minimize volume-scavenging effects. Specifically, all droplet-to-droplet fluid communication must travel through the flow-restricting porous pump layer. Any gaps between the pump and the top plate must be eliminated so that holes are isolated from one another and directly contact the top surface of the pump. In SW devices, this requires sanding the top layer of the glass frit to a flat surface to ensure good mating to the top plate. In MS devices, rubber gaskets and the top electrode have identical hole patterns to the top plate and the devices are assembled with these layers carefully aligned. Order of assembly is top plate, gasket, electrode plate, gasket, pump surrounded along sides by gasket, electrode, gasket, bottom plate/reservoir.

The principle of rapid reconfiguration of small-scale droplet shapes in response to low voltage pulses is the same here as with the electroosmotic droplet switch (EODS) (1, 2), although the present device utilizes a monolithic array of droplets that share a common pump with a single shared reservoir that replaces the "bottom" droplets in the EODS.

Device characteristics. The hole arrays cover an area roughly 15 mm × 15 mm. SW devices are compact in thickness, with top and bottom silicon wafers of 400 μm thickness each plus 1.5–3 mm pumping layers. MS devices have top plates of 3 mm thickness, 4 mm pumping layer, and a large (25 mm) bottom plate. Hole sizes ranged from $\epsilon = 150$–900 μm, and the number of holes ranged from $N = 100$–4876. The tightest hole packing tested ($\phi = 0.4$) was sufficient for the liquid bridges to remain isolated from each other. The reservoir in SW devices was etched out (depth of approximately 150 μm) of the inner surface of the bottom plate with an array of small pillars left standing to support the pumping material.

Working fluid and pump. The working fluid in this paper is untreated commercial distilled water (Poland Springs), and the pumping materials are off-the-shelf porous glass frits, used as provided. Although we have previously tested well-characterized fluids and pumps to quantify electroosmosis (3), we find the present system (untreated commercial distilled water and porous glass discs) performs well, with a zeta potential of nearly 100 mV (based on in-house characterization) and minimal signs of pump strength deterioration over time. Frits with "very fine" porosity (Robu, $R_{\text{nominal}} = 1.3$ μm) are sufficient for pumping against droplets down to $\epsilon = 300$ μm at 10 V and are used in the present study. Other materials with sufficiently fine pores, even with a reduced zeta potential, can pump against smaller droplets. See Table S1 for typical values of material properties and geometric parameters.

Surface tension measurements. Surface tension measurements were made in a separate system by a standard pendant drop technique (4). Several surface tension measurements were made in this way for both fresh (unused) water as well as water that had just been used in an experiment. Fresh water measurements agreed with literature values (≈72 mN/m), validating the technique.

Contact line pinning. Contact lines of the droplets/bridges are fixed along the corner of the circular orifice by a combination of geometry and chemistry. The outer surfaces of the SW devices are coated with an antistiction monolayer of FOTS (fluoro-octyl-trichloro-silane) via molecular vapor deposition (reported contact angle with water $\theta_e \approx 110°$). The MS devices rely on lips around the orifice produced by a prescribed drilling protocol to pin the contact line; details will be reported elsewhere.

Holding capacity tests. The substrate-pendant (Fig. 1*B*) and device-pendant (Fig. 1*C*) tests provide checks on predictions of holding capacity. The MS-fabricated device in Fig. 1*B* has a predicted capacity of 1020 mg ($N = 100$, $\epsilon = 440$ μm, clean water). The device holds a variety of substrates (Fig. 1*D*) with masses in the range of 630–725 mg until EO-activated detachment is called for. Holding times exceeding ten minutes have been observed. The only qualitative difference between tests with different substrates is a longer voltage detachment pulse needed for the rougher substrates, perhaps due to penetration of water into these more porous substrates. The SW-device has a predicted adhesion capacity of 8.4 g ($N = 1219$, $\epsilon = 300$ μm). This device is able to hold its own wet weight of 4.3 g (no battery or controls on-board). For these quantitative tests, details of reservoir closure influence the adhesion. Fig. 3*A* (*Inset*) illustrates how the reservoir liquid may be open to the atmosphere ("atmospheric adhesion") or closed-off via the 3-way valve ("closed adhesion").

Operation notes. In device-pendant mode, tests were made without on-board power supply and control circuit. For some tests, thin wires (carefully aligned to not impart a force on the hanging device) connect the device to the power supply. For other tests, the electrical leads to the power supply are taped to the substrate to allow contact with flexible interconnects attached to the device electrodes. The device is held by hand against the substrate until liquid contacts are made, and then allowed to hang by its own strength.

Scavenging. The adhesion device can be affected by "volume-scavenging," where a curvature (pressure) difference between drops/bridges drives flow, resulting in undesired volume redistribution (5). In the SECAD, this can greatly reduce contact perimeter through coalescence of the bridges. The scavenging effect is most active during initial droplet-to-substrate contact when the attachments may not be precisely synchronized. One way to mitigate this effect is to enhance flow resistance between bridges. In the SECAD, this is done with the middle layer that plays dual roles: EO pump and retarder of scavenging. The condition for minimizing scavenging is the same as for a strong pump ($\mathcal{S} \gg 1$).

Free Energy Decrease. To the extent that liquid/gas interfacial area dominates the free energy of the device as a thermodynamic system, the tendency toward coalescence follows the tendency

toward lower free energy. Mitigating coalescence (Fig. 2*B* and Fig. 3*B*) requires precise metering by the pump, maintaining the integrity of the N contact lines and avoiding volume-scavenging. These are the challenges we face at present in our lab in using a face-pad with $N = 10,000$ holes of $\epsilon = 10$ μm.

Control. The final equilibrium configuration of the capillary surfaces can be influenced by constraining the pressure or volume of the device, controlled by the valve shown in Fig. 3*A* (*Inset*). Present experiments typically probe "atmospheric adhesion" (the device is connected to a large free surface at the same height as the droplets). This ensures that droplets or bridges will relax to zero-mean-curvature shapes (i.e., pieces of catenoids for bridges, or flat surfaces for droplets). A syringe is used to manually control volumes for some experiments; in this case the three-way valve in Fig. 3*A* (*Inset*) is switched to the free surface immediately after the liquid contacts are made. The valve also permits the system to be "primed" before experiments by temporary (approximately 5 s) elevation of the free surface. When the droplets equilibrate to this hydrostatic pressure, they are uniform in shape and height, resulting in better adhesion.

Equilibrium and Stability. An array of capillary surfaces with equal pressures (e.g., all identical droplets or identical bridges) is an equilibrium state, but not necessarily a stable one as seen by two coupled superhemispherical droplets in (1). However, for the configurations observed in the SECAD (all subhemispherical droplets, all short near-cylindrical bridges, or a combination of the two), we do expect stability. Note that similar experiments were left in the "attached" state for longer than shown in Fig. 3*A* and those experiments do reach a steady value of adhesion force.

Bridge Height Variation. The value of bridge height (α) was varied for some experiments with no systematic variation in adhesion strength detected. This observation supports the claim that the Young–Laplace pressure contributions are insignificant relative to perimeter forces for "atmospheric adhesion." Slight systematic variation is expected due to differences in substrate-side contact diameter, but these variations are smaller than the noise in the data.

Although the final equilibrium adhesion force is the same for different values of α, the dynamics of grab and release are slightly different, as can be seen by comparing Fig. 3*A* with Fig. S1. For the shorter bridges in Fig. S1 (also see Movie S4), a shorter "attach" pulse (80 ms) is sufficient for grabbing and a longer "release" pulse (500 ms) is required. Also, the equilibration time scale seems longer and other subtle differences are apparent, such as the small bump during attachment. Note that in Movie S4 the two bridges in the lower left corner coalesce due to overfilling (discussed in *Materials and Methods: Data Normalization*). Such small regions of coalescence seem to be stable and have minimal effect on overall adhesion strength.

Switching Time Approximation. τ is switching time from detached state (approximated as zero-volume droplets level with the orifice) to attached state (approximated as cylindrical bridges), and switching time is estimated from total volume divided by EO flow rate [Smoluchowski approximation; see (1)]. For porous pumps used here, we assume to first order that the full area of the pump contributes to flow because the porous structure allows for lateral flow from the area between holes in the top plate. For a pumping structure with isolated pores (e.g., alumina membranes), the pumping area would be limited to the area directly beneath the holes, so the expression for τ should be modified by removing the factor of ϕ.

A comparison of experimental results to this prediction ($\tau \equiv \frac{\epsilon\phi\mu\alpha L}{\psi|e\zeta V|}$; see manuscript or Table S1 for definitions) is shown in Fig. S2. Here the measured τ is the time from the start of the voltage pulse to the moment that the first droplet makes contact with the substrate.

Geometric Factor (β) Approximation (In Definition for Pump Strength $\mathcal{S}$). The maximum capillary pressure that the pump must overcome can be written as $4\beta\sigma/\epsilon$. It represents the maximum pressure due to surface tension. For pumping droplets in and out of a hole of diameter ϵ (in the absence of a substrate, e.g., Fig. 2*B*), β is bounded by the hemispherical capillary pressure ($\beta \leq 1$). In contrast, when bridges exist (in the presence of a substrate), β can be considerably larger than unity and represents the maximum mean curvature that exists during a grab/release cycle. In this sense, it is a geometric parameter.

$\beta = 1$ for bridges of height $\alpha > 0.15$ where the greatest capillary resistance is during "grab," approximated as hemispherical droplet. For shorter bridges, the greatest resistance is during detachment due to large-curvature in bridges and $\beta \approx 1/(4\alpha)$, assuming $\theta_c = 90°$. The longer "release" pulses in Fig. 3*A* and Fig. S1 are due to this capillary resistance to EO pumping.

Amplification by Shape Suction. Considerable improvements over atmospheric adhesion may be possible by exploiting the shape suction resulting from negative pressures within the bridges. As an upper bound of this curvature, we consider a concave bridge with a semicircular profile (tangent to the substrate and top plate). Based on these curvatures, the total adhesion strength is increased by a factor of $(\frac{1}{\alpha} - 1)/2$. The suction bonus is unbounded as bridge height goes to zero, but for a bridge with height : diameter ratio of 1 : 6 as in Fig. 3, the prediction is for a 2.5-fold increase in adhesion strength. A tenfold amplification corresponds to a short bridge of $\alpha \approx 1/20$.

Pumping Material Limitations. The glass frit presently used for EO pumping ($R \approx 1.3$ μm) becomes too weak to pump droplets smaller than $\epsilon \approx 300$ μm ($\mathcal{S} \sim 1$) at small voltages. This explains the higher voltage (40 V) used in Fig. 3. Alternate pumping materials have been successfully tested in our lab and have been reported by others. Anodic alumina and polymer membrane filters have smaller zeta potentials (10–40 mV), but are available with pore size down to 10 nm, which is sufficient for fast pumping in the present application (6, 7). Also, coating similar membranes with a layer of silica has been shown to further increase the strength of the pump by increasing the zeta potential (8). This last point provides the justification for scaling of τ in Table 1.

The scaling example in Table S2 provides more detail regarding pump scaling. Here, a glass frit similar to that used in the present experiments is used for $\epsilon \geq 300$ μm, and an alumina porous disc is used for $\epsilon < 300$ μm. Despite a smaller zeta potential, the alumina pump is stronger not only due to its finer pore size, but also due to its stronger electric field (same applied voltage over a much thinner pump). The smallest holes listed in Table S2 cannot be pumped by over-the-counter pumping materials that we are aware of, though an electroosmotic pump should still be possible through materials modifications or alternate fabrication processes [e.g., (8)]. Note that some degradation of electroosmosis due to electric double layer overlap in smaller pores is expected but not considered in the table.

1. Vogel, M. J., Ehrhard, P. & Steen, P. H. The electroosmotic droplet switch: Countering capillarity with electrokinetics. *Proc Natl Acad Sci USA* 102, 11974–11979 (2005).
2. Steen, P. H., Ehrhard, P. & Vogel, M. J. (2006). *USA patent* application #11/496,242, filed 31 July2006.
3. Barz, D. P. J., Vogel, M. J. & Steen, P. H. Determination of the zeta potential of porous substrates by droplet deflection: I. the influence of ionic strength and ph value of an aqueous electrolyte in contact with a borosilicate surface. *Langmuir* 25, 1842–1850 (2009).

4. Fordham, S. On the calculation of surface tension from measurements of pendant drops. *Proc R Soc* A 194, 1–16 (1948).
5. van Lengerich, H. B., Vogel, M. J. & Steen, P. H. Dynamics and stability of volume-scavenging drop arrays: Coarsening by capillarity. *Physica* D 238, 531–539 (2008).
6. Chen, Y.-F., Li, M.-C., Hu, Y.-H. & Chang, C.-C., W.-J.and Wang. Low-voltage electroosmotic pumping using porous anodic alumina membranes. *Microfluid Nanofluid* 5, 235–244 (2007).
7. Gupta, A., Denver, H., Hirsa, A. H., Stenken, J. & Borca-Tasciuc, D.-A. Localized, low-voltage electroosmotic pumping across nanoporous membranes. *Appl Phys Lett* 91, 094101 (2007).
8. Vajandar, S. K. et al. SiO_2-coated porous anodic alumina membranes for high flow rate electroosmotic pumping. *Nanotechnology* 18, 275705 (2007).

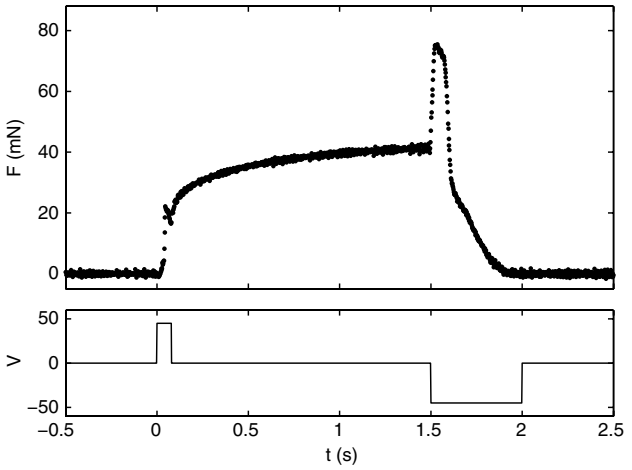

Fig. S1. Force-transducer experiment for $\alpha = 0.05$. Compare to Fig. 3*A*. Force (*Upper Plot*) felt by substrate over time due to voltage pulses applied (*Lower Plot*). Also see Movie S4. Device has $\epsilon = 500$ μm, $N = 448$, $\phi = 0.4$.

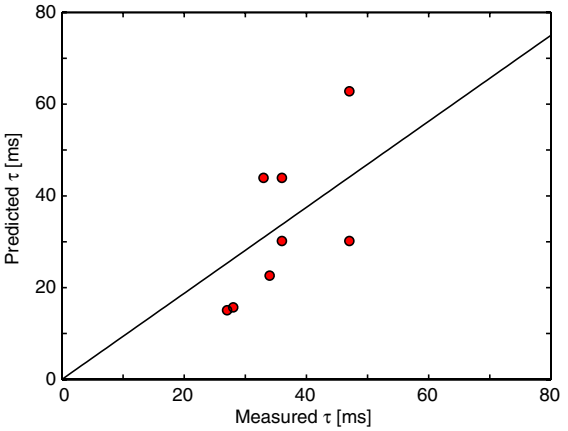

Fig. S2. Comparison of time-to-switch τ: Measured versus predicted values.

Movie S1. Reversible wet adhesion: Demonstration of concept in substrate-pendant mode. First substrate (Plexiglas) is 2 cm × 2 cm. The voltage pulse to attach is displayed on the oscilloscope (grab/release pulses are ±15 V). Note footprints left on Plexiglas substrate after release. Device is MS (machine shop), $N = 10 \times 10$, $\epsilon = 440$ μm.
Movie S1 (MPG)

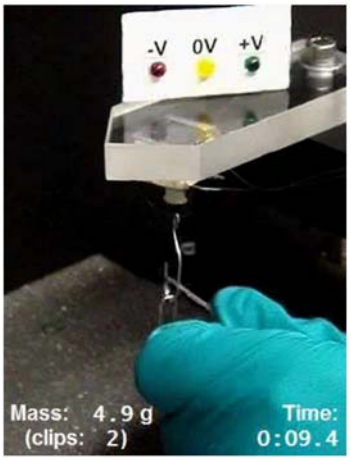

Movie S2. Reversible wet adhesion: Demonstration of concept in device-pendant mode. LEDs show voltage pulses ($V \approx 20$ V). Device is SW (silicon wafer), $N = 1219$, $\epsilon = 300$ μm.
Movie S2 (MPG)

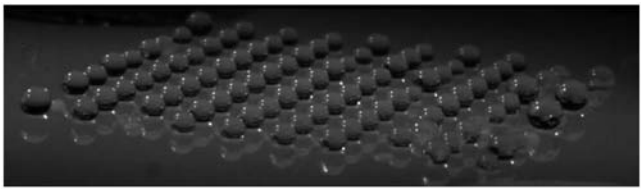

Movie S3. Operation of device with no substrate present. Movie playback is real-time. Device is MS (machine shop), $N = 10 \times 10$, $\epsilon = 440$ μm, $V \approx 12.5$ V.
Movie S3 (MPG)

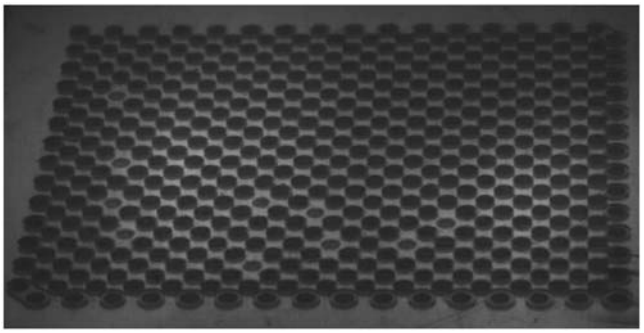

Movie S4. Grab and release dynamics of SECAD, corresponding to experiment in Fig. S1. View is through Plexiglas substrate, as shown in Fig. 3*A* (*Inset*). Movie playback is real-time. Device is SW (silicon wafer), $N = 448$, $\epsilon = 500$ μm, $V \approx 40$ V. The array of holes is ≈16 mm wide.
Movie S4 (MPG)

Table S1. Typical values of material properties and geometric parameters for the present experiments

	Typical value	Description
ϵ	150–900 mm	Hole diameter
N	100–5000	Number of holes
ϕ	0.1–0.4	Packing density
α	$0.05L - 0.3L$	Spacer height
V	5–40 V	Voltage drop
ζ	-0.1 V	Zeta potential
e	710 pF/m	Electric permittivity
β	1	Geometric factor
R	1.3 μm	Pump pore radius
L	0.2–3 mm	Pump thickness
ψ	0.25–0.4	Pump porosity
σ	55 mN/m	Surface tension
μ	10^{-3} Pa s	Viscosity
θ_c	68°	Contact angle

Table S2. Device scaling. Based on device with area 1 cm^2, hole packing $\phi = 0.5$, bridge height $\alpha = 0.25$, voltage drop across pump $V = 10$ V, clean water $\sigma = 72$ mN/m, and atmospheric adhesion. "SiO_2" pump is 1 mm thick, with $\zeta = 100$ mV, mean pore radius $R = 1.5$ μm, and porosity $\psi = 0.3$. "Al_2O_3" pump is 120 μm thick, $\zeta = 40$ mV, $R = 10$ nm, and $\psi = 0.4$

	Pump scaling			Adhesion scaling		
Hole size ϵ(μm)	Material	Strength $\mathcal{S}$	Switch time τ (ms)	N	Strength (N/cm^2)	Capacity (g)
1000	SiO_2	6.4	570	64	0.013	1.3
500	SiO_2	3.2	290	250	0.026	2.7
300	SiO_2	1.9	170	710	0.044	4.4
100	Al_2O_3	8000	13	6400	0.13	13
10	Al_2O_3	800	1.3	6.4×10^5	1.3	130
1	Al_2O_3	80	0.13	6.4×10^7	13	1.3 kg
0.1	Al_2O_3	8	0.013	6.4×10^9	130	13 kg
0.01	—	—	—	6.4×10^{11}	1300	130 kg